

Comparison of Measured and Predicted Flows through Conical Supersonic Nozzles, with Emphasis on the Transonic Region

L. H. BACK,* P. F. MASSIER,† AND H. L. GIER‡

Jet Propulsion Laboratory, California Institute of Technology, Pasadena, Calif.

To understand better equilibrium flows through supersonic nozzles, wall static pressures have been measured in nozzles with circular-arc throats having different ratios of throat radius of curvature to throat radius r_c/r_{th} , circular-arc or conical convergent sections, and conical divergent sections. These measurements were made with air at stagnation temperatures of 530° and 1500°R and over a stagnation pressure range from 45 to 250 psia. The flow through the transonic region was found to depend essentially on local configuration, i.e., on the ratio r_c/r_{th} ; two-dimensional isentropic flow predictions agreed with the data in this region for the nozzles with $r_c/r_{th} = 2.0$, but were inadequate for the nozzle with $r_c/r_{th} = 0.625$. By comparison, the simple one-dimensional isentropic flow prediction was as much as 45% high in the throat region for one nozzle; in the conical sections, deviations of a smaller magnitude were found. The effects of wall cooling and variation in the boundary-layer thickness at the nozzle inlet were investigated, as were differences in pressure readings with taps of various sizes. Some separation pressure data are presented to show the effect of wall cooling. Other flow features that indicate the extent of deviations from one-dimensional flow include flow coefficients, thrust ratios, and local mass fluxes. It is hoped that these comparisons between measurements and predictions will be useful in studying nozzle flows with the additional complexity of chemical reactions.

Nomenclature

a	= speed of sound
a^*	= speed of sound at the sonic condition
A	= local nozzle cross-sectional area
A_{th}	= nozzle-throat area
C_d	= flow coefficient
d	= static-pressure tap diameter
D	= nozzle-inlet diameter
F	= axial thrust
l	= nozzle approach section length
\dot{m}	= mass flow rate
M	= Mach number
p	= wall static pressure
p_a	= ambient pressure
p_s	= separation pressure
p_t	= stagnation pressure
r	= nozzle radius
r_{th}	= nozzle-throat radius
r_c	= nozzle-throat radius of curvature
r_i	= nozzle-inlet radius of curvature
R	= nozzle-inlet radius
T_t	= stagnation temperature
T_w	= wall temperature
z	= axial distance from nozzle inlet
u	= velocity component in z direction
V	= flow velocity at wall
γ	= specific-heat ratio
δ	= velocity boundary-layer thickness at nozzle inlet
δ^*	= displacement thickness
ϵ_c	= nozzle contraction-area ratio
ϵ_E	= nozzle expansion-area ratio
ν	= kinematic viscosity
ξ	= distance defined in Eq. (6)
ρ	= density
τ	= wall shear stress

Subscripts

e	= condition at freestream edge of boundary layer
i	= condition at nozzle inlet

s	= condition at flow separation
t	= stagnation condition
1	= one-dimensional flow value

I. Introduction

Flows through supersonic nozzles are of interest in design and development and in basic research. In the applied field, nozzles are used in rocket engines and in measuring flow rates, whereas in research they are used in acceleration devices and in the study of flow phenomena such as non-equilibrium effects. This experimental investigation was initiated to gain a better understanding of equilibrium flows through nozzles which appears to be basic in studying the additional effects associated with chemical reactions. Data are presented through the subsonic, transonic, and supersonic flow regions of a number of conical nozzles. Emphasis is placed on the throat region, where the flow is transonic.

Previous investigations of gas flows through conical nozzles have shown deviations from one-dimensional isentropic flow, as indicated by measured wall static pressures. These deviations result from radial velocity components caused by the taper and curvature of the nozzle.¹ Similar deviations have been observed where measurements were made in the divergent region of conical nozzles²⁻⁵ and where a few measurements were made in the conical convergent region.⁶ Local velocity measurements⁷ in the throat region have indicated the two-dimensionality of the flow.

In this paper, measured wall static pressures are presented for conical nozzles of various dimensions to show in detail those regions where the flow is two-dimensional, and thus where the simple one-dimensional flow prediction fails. The conical nozzles investigated have 30° and 45° half-angles of convergence, 15° half-angles of divergence, circular-arc entrance and throat sections, and expansion-area ratios up to 6.6. The ratios of throat radius of curvature to throat radius were 2.0 and 0.625. The effect of inlet configuration was investigated in other nozzles with the convergent sections formed by circular arcs.

Operating conditions spanned stagnation pressures from 45 to 250 psia and stagnation temperatures from 530° to 2000°R, with data reported at 530° and 1500°R. The ambient pressure was atmospheric. At the lower stagnation

Received September 8, 1964; revision received May 17, 1965. This paper presents the results of one phase of research carried out at the Jet Propulsion Laboratory, California Institute of Technology, under Contract No. NAS 7-100, sponsored by NASA.

* Senior Research Engineer.

† Research Group Supervisor. Member AIAA.

‡ Research Engineer; now graduate student at the University of Colorado.

temperature of 530°R, compressed air was used, and the nozzles were uncooled. The higher stagnation temperatures were obtained by heating compressed air by the combustion of methanol. The products of combustion were then mixed to obtain uniformity before entering the nozzles, and at these higher temperatures, the nozzle walls were cooled. At the highest stagnation temperature, the total heat transfer from the gas to the nozzle wall was less than 1% of the total energy of the gas at the nozzle inlet so that the flow was nearly adiabatic in all cases. The products of combustion could be treated approximately as air, since the mass flow-rate ratio of methanol to air was small, e.g., at 1500°R the molecular weight and specific-heat ratio were 28.6 lb/mole and 1.34, respectively, for the products of combustion compared with 29.0 lb/mole and 1.35 for air. Also, calculated temperatures of the products of combustion, with the assumption of complete chemical reactions, were within the accuracy of thermocouple measurements described in Sec. II.

Boundary-layer thicknesses at the nozzle inlet were varied from about 5 to 45% of the inlet radius to investigate boundary-layer displacement effects. The effect of wall static-pressure tap size on the readings was also investigated. At the lower stagnation pressures, the nozzles were overexpanded, and the associated separation pressures are presented both for hot-flow operation with cooled walls and for cold-flow operation. Other features of the flow are included in terms of deviations from one-dimensional isentropic flow. For over-all nozzle performance, flow coefficients and thrust ratios are shown. Local deviations in the mass flux at the edge of the boundary layer calculated from the measured wall static pressures are included, as is the sonic line location.

In the transonic flow region, various two-dimensional isentropic flow predictions are compared with the data to indicate the adequacy of these theories.

II. Instrumentation

The flow and instrumentation diagram of the system to which the nozzles were attached is shown in Ref. 1. Stagnation pressure was measured just upstream of the approach section, the length of which could be adjusted to specified values. Changes in length were made to vary the nozzle-inlet boundary-layer thickness. These turbulent boundary-layer thicknesses were estimated from measurements described in Ref. 1. The approach section was cooled at the higher stagnation temperature of 1500°R. Stagnation temperature was determined by averaging the readings of two shielded thermocouples placed 0.25 in. upstream of the nozzle inlet. These two thermocouples, located 1 in. from the centerline, were spaced 180° apart circumferentially and generally read within 2% of each other. The air mass flow rate was measured with an orifice, and for the hot-flow tests, a rotometer was used to measure the mass flow rate of methanol. The accuracy of the total mass flow rate is estimated to be 1% at stagnation pressures above about 100 psia. At lower stagnation pressures, the readings are less accurate.

For the following nozzles [the 30°-15° (Fig. 1), those shown in Fig. 2, and the 45°-15° (Fig. 3)], the diameters of the wall static-pressure taps were 0.040, 0.020, and 0.020 in., respectively, and the ratios of hole depth-to-diameter were about 8, 4, and essentially infinity, respectively. The holes were as sharp-edged as they could be made by drilling and then smoothing the burrs with emery cloth. The axial location of each tap was known to 0.002 in., and the taps were spaced circumferentially and axially along each nozzle wall. The static pressures were measured either with mercury manometers or, at the higher pressures, with Heise gages, which had 0.25-psia marked increments. The accuracy of the readings is dictated by the difference between the static and stagnation pressures and thus depends on location in the nozzle and on the stagnation pressure. The estimated error in static pressure throughout the throat and

divergent regions and most of the convergent region is less than 1%. Only in the nozzle-inlet region at the lowest stagnation pressures, where the difference between the static and stagnation pressure is small, is the estimated error of 5% significant; this error would be less at higher stagnation pressures. Considerably larger differences than the previously mentioned 1% through most of the nozzle are found with different sized taps, as discussed in Sec. V.

For hot-flow operation with cooled walls, wall temperatures were determined from thermocouples embedded in the wall of the 30°-15° nozzle and from calorimetric wall heat-flux measurements with the 45°-15° nozzle.

III. Static-Pressure Distributions

Measured static-to-stagnation-pressure ratios are shown in Fig. 1 for the 30°-15° nozzle over a range of stagnation pressures from 45 to 150 psia at a stagnation temperature of 1500°R, with cooled walls. The upper limit of 150 psia was dictated by manometer limitations at the time the tests were made. From boundary-layer traverses, the ratio of inlet boundary-layer thickness to nozzle-inlet radius was estimated at about $\delta/R \approx 0.25$. The pressure ratios are nearly invariant with stagnation pressure except in the flow-separation region, where the rise in static pressure is caused by overexpanded nozzle operation. In the throat region, there is some data spread, but it does not appear to vary systematically with stagnation pressure. Considerable deviations from the prediction for one-dimensional (1-*d*) isentropic flow ($\gamma = 1.40$), shown as curve *a*, are apparent in the transonic region; in particular, the measured pressures are as much as about 30% below the prediction just downstream of the throat. Deviations of a smaller magnitude are observable in the inlet and conical convergent section, where the data are slightly above the 1-*d* flow prediction. Near the tangency of the circular-arc throat and conical divergent section, the measured pressure ratios change slope abruptly and cross over the 1-*d* flow prediction further downstream. A 1-*d* isentropic flow prediction with variable specific heat was also made and found to be at most 2% above the prediction shown for $\gamma = 1.40$. This small difference indicated the prediction with $\gamma = 1.40$ to be adequate for comparison purposes if the entire nozzle flow region is considered. For subsequent comparisons in the throat region, γ differs little from the stagnation condition value of 1.35 used.

Another 1-*d* flow prediction referred to in the literature is that for conical source flow in the divergent region. The predicted wall static-pressure distribution for isentropic flow ($\gamma = \text{const}$) is

$$\frac{p}{p_b} = \left\{ 1 - \frac{\gamma - 1}{2} M_b^2 \left[\frac{(s_b/s)^4}{(p/p_b)^{2/\gamma}} - 1 \right] \right\}^{\gamma/(\gamma-1)} \quad (1)$$

The subscript *b* denotes a point along the conical wall where the indicated variables are known, and *s* is the radial distance from the source. If the experimental pressure and corresponding Mach number at the circular-arc-throat conical tangency point are used, Eq. (1) is shown in Fig. 1 by curve *b* to predict substantially lower static pressures in the conical section than those obtained experimentally. Although better agreement could be obtained if the prediction were initiated downstream of the tangency, the comparison nevertheless indicates that the actual flow differs from conical source flow in the first part of the conical section.

Data were also obtained both at a lower stagnation temperature of 530°R (uncooled walls) and with no approach length such that at the nozzle inlet $\delta/R \approx 0.05$. These data, though not shown, indicated that the effect of wall cooling altered the measured pressure ratio negligibly except in the flow-separation region, where, at the same stagnation pressure, the separation point moved downstream with wall cooling. The dependence of separation pressure on wall

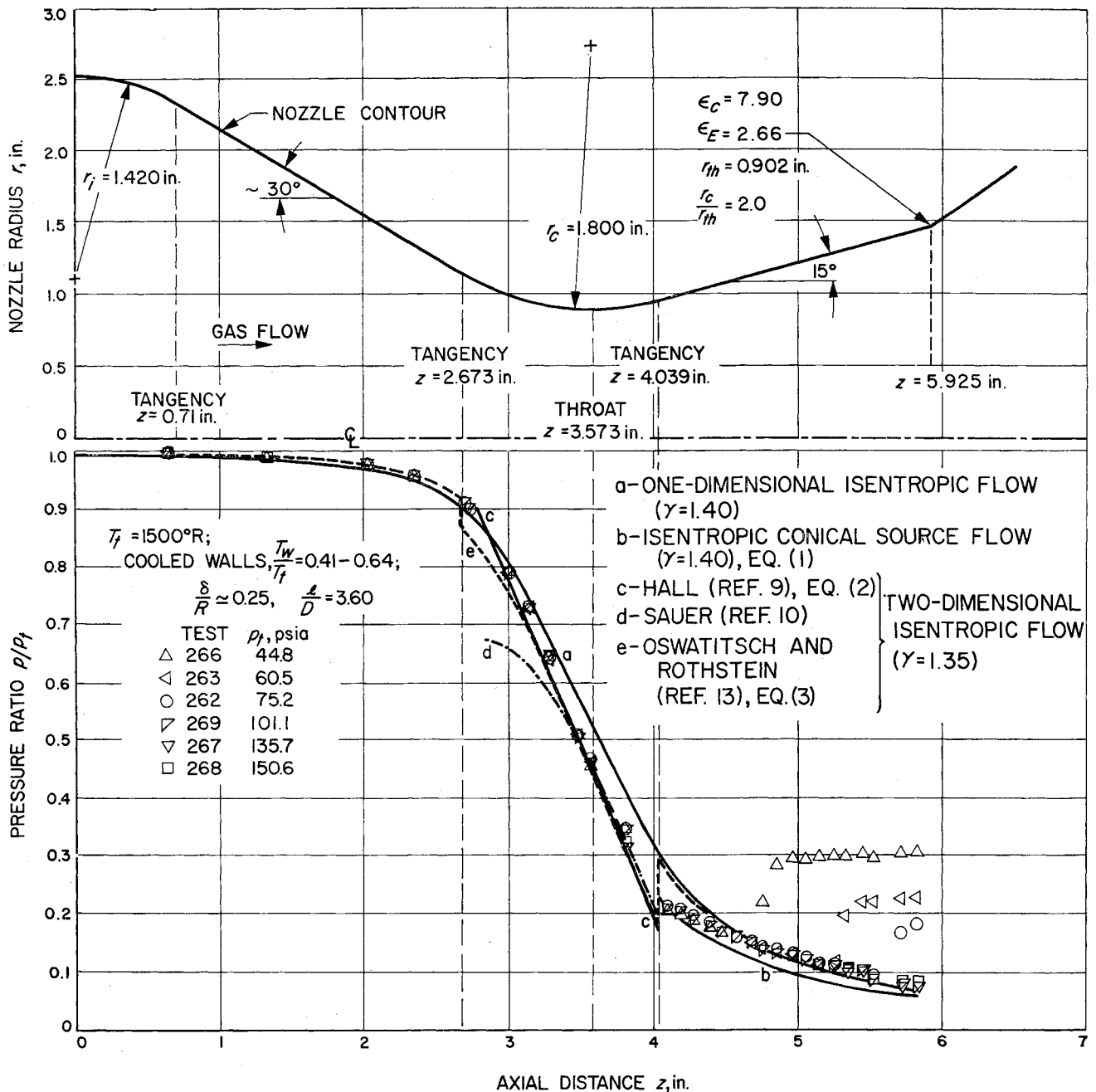


Fig. 1 Static-to-stagnation-pressure ratios along the 30°-15° nozzle.

cooling is discussed in Sec. VI. The effect of inlet boundary-layer thickness on the measured pressure ratio was not discernible. Thus these investigations revealed a negligible boundary-layer displacement effect, which was also in agreement with predictions of the displacement thickness δ^* from the turbulent boundary-layer analysis.⁸ In connection with the prediction, it should be mentioned that δ^* became negative upstream of the throat as a result of the combined effects of wall cooling and flow acceleration. Predicted values of δ^* are shown in Fig. 12 of Ref. 1.

To investigate the effect of inlet configuration, measured pressure ratios are shown in Fig. 2 for nozzles of different contraction-area ratios but having the same throat radius, throat radius of curvature, and half-angle of divergence. The convergent sections were formed by circular arcs of equal radii of curvature. For comparison purposes, the cold-flow data shown are average values for each nozzle over the range of stagnation pressures indicated. Separated flow data (not shown) are discussed in Sec. VI. Through the throat and divergent regions, the measured pressure ratios are essen-

tially independent of inlet configuration and depend only on the local nozzle contour. The magnitudes of the deviations from 1-d isentropic flow (curve a) are similar to those found with the 30°-15° nozzle (Fig. 1), which has the same ratio of throat radius of curvature to throat radius ($r_c/r_{th} = 2.0$) and half-angle of divergence as the nozzles shown in Fig. 2.

The effect of throat configuration is shown by comparing Fig. 3 to Fig. 1. In Fig. 3, measured pressure ratios for the 45°-15° nozzle are shown for a stagnation-pressure range from 45 to 250 psia and a stagnation temperature of 1500° R. Because of the smaller throat radius of curvature to throat radius of 0.625, as compared to 2.0 for the 30°-15° nozzle, there are larger deviations from the pressure ratio for 1-d isentropic flow in the transonic region. These amount to as much as 45% just downstream of the throat. In the conical convergent section, there are also larger deviations from 1-d flow than with the 30°-15° nozzle because of the larger 45° half-angle of convergence. In addition, at the higher expansion-area ratios of the 45°-15° nozzle, the data once more cross over and become less than the 1-d flow pre-

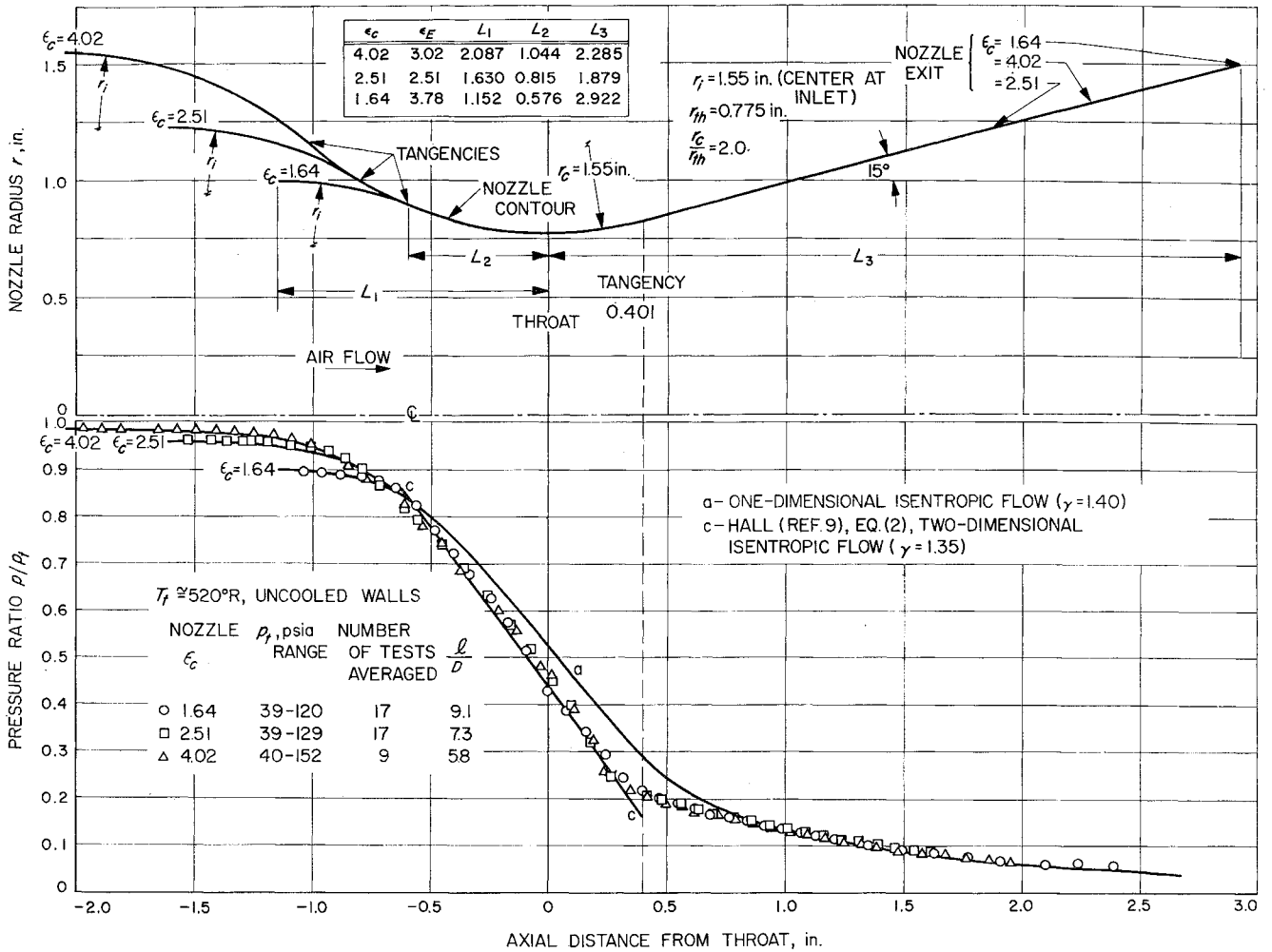


Fig. 2 Static-to-stagnation-pressure ratios with various nozzle-inlet configurations.

dition. With the 45°-15° nozzle, only hot-flow cooled-wall data were obtained, and a larger upstream length ($l/D = 8.4$) was used such that $\delta/R \approx 0.45$. Although no data were obtained with a thinner inlet boundary-layer thickness, both experimental observations with the 30°-15° nozzle and predictions indicate that the measured pressure ratios would be altered negligibly.

IV. Two-Dimensional Flow Predictions

Exact solutions of the two-dimensional (2-d) isentropic-flow equations are virtually nonexistent for flow regimes throughout a supersonic nozzle. Approximate solutions consist either of calculating the flow field by numerical or graphical techniques or of obtaining analytical solutions in particular flow regions. Since, as expected, deviations from 1-d flow are largest near the throat, the transonic region is of primary concern. Also, a solution in this region is needed to initiate a solution by the method-of-characteristics in the supersonic region.

In the transonic region, Hall⁹ obtained a solution for the velocity field for isentropic, irrotational flow ($\gamma = \text{const}$) by a series expansion of the velocity components in inverse powers of r_c/r_{th} . The first three terms for the velocity components in the series solution were calculated and appear in the reference. From these, the wall static-to-stagnation-pressure ratio can be calculated:

$$p/p_t = \{1 - [(\gamma - 1)/(\gamma + 1)]\bar{V}^2\}^{\gamma/(\gamma-1)} \quad (2)$$

where \bar{V} is the local velocity V at the wall, nondimensionalized with respect to the speed of sound at the sonic condition

α^* . The prediction from Eq. (2) is shown in Fig. 1 by curve c , which agrees well with the measured pressure distributions in the throat vicinity. In the regions that extend to the circular-arc-throat conical tangencies, the requirement that the velocity at the wall be parallel to the wall is not exactly satisfied as a consequence of the solution method; this undoubtedly leads to the inferior prediction near these tangencies.

The correspondence of the prediction from Eq. (2) with the data is equally good for the nozzles with various inlet configurations, as shown in Fig. 2 by curve c . It should be noted that Hall's prediction depends only on throat configuration through the ratio r_c/r_{th} and not on inlet configuration. The measured pressure ratios in the throat region shown in Fig. 2 display this same trend.

For the 45°-15° nozzle ($r_c/r_{th} = 0.625$), the prediction is not applicable since the series solution diverges for $r_c/r_{th} < 1$. Instead, Fig. 3 shows as curve d the Sauer prediction,¹⁰ which, as Hall has pointed out, is the first-term approximation in his series solution. This prediction is considerably below the data for the 45°-15° nozzle. In Fig. 1 (curve d), this prediction indicates the improvement upstream of the throat afforded by the Hall solution, curve c , in which three terms are used. However, at the throat and downstream of it, there is little difference between the first and third approximations.

It would be of interest to compare the data with predictions from the irrotational method of characteristics in the supersonic region; however, predictions by Darwell and Badham¹¹ and Migdal and Landis¹² for conical nozzles with circular-arc throats reveal flow conditions near the nozzle

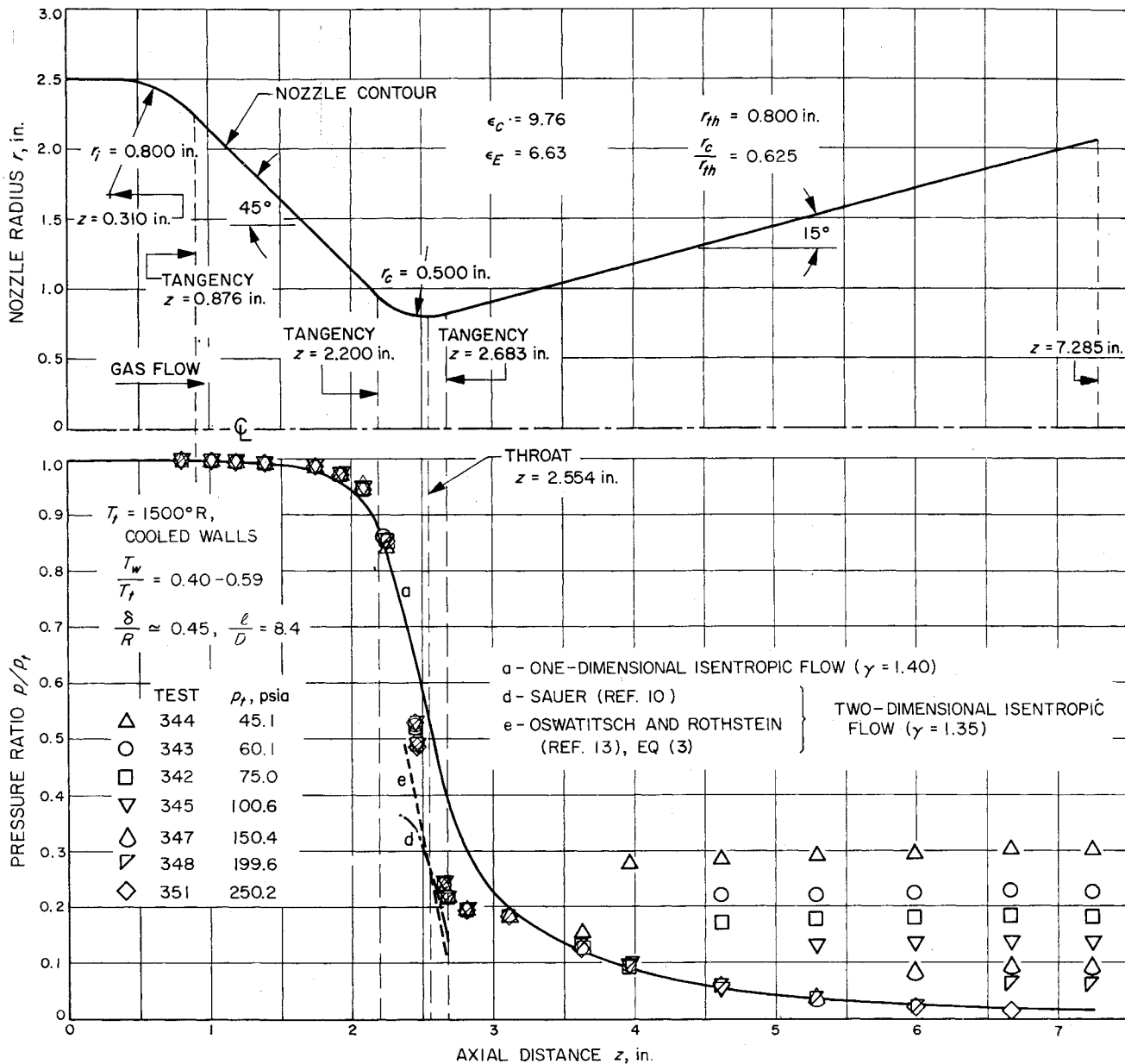


Fig. 3 Static-to-stagnation-pressure ratios along the 45°-15° nozzle.

axis that would lead to shock formation, and consequently invalidate the irrotational assumption. Predicted shock formation occurs where Mach lines originating just downstream of the circular arc and conical tangency approach the nozzle axis. Darwell and Badham discuss the prediction in detail with respect to the accuracy of the numerical solution and its initiation, using either Hall's⁹ or Sauer's¹⁰ transonic solution. As indicated in Fig. 1, for the 30°-15° nozzle with $r_c/r_{th} = 2.0$, either of these solutions should provide a good approximation to the actual flow in the region of interest. It should be noted that boundary-layer displacement effects, not accounted for in these predictions, do influence the nozzle freestream flow boundary to some extent; this can alter the predicted flow field. Whether or not shock formation actually occurs along the nozzle axis can only be decided by experimental observation. Rather than wall static-pressure measurements, either total pressure-probe traverses along the axis of conical nozzles or some means of visual observation in a transparent nozzle with a sufficiently long divergence section would be required.

Another approximate solution valid throughout the nozzle, providing that wall curvature effects are not large, is the pre-

diction by Oswatitsch and Rothstein.¹³

$$\frac{p}{p_t} = \left[1 - \frac{\gamma - 1}{2} \left(M_1 \frac{a_1}{a_t} \right)^2 \left(\frac{V}{u_1} \right)^2 \right]^{\gamma/(\gamma-1)} \quad (3)$$

where

$$\frac{V}{u_1} = \left[\left\{ 1 + \frac{1}{2} \left[\frac{r}{2} \frac{d^2 r}{dz^2} + \frac{1}{4} \left(\frac{du_1/dz}{u_1} \right) r \frac{dr}{dz} - \left(\frac{dr}{dz} \right)^2 \right]^2 + \left(\frac{dr}{dz} \right)^2 \right\}^{1/2} \right]$$

The subscript 1 denotes average quantities for 1-d isentropic flow, in which $\gamma = \text{const}$. For calculation purposes, it is convenient to use the relation $(1/u_1)(du_1/dz) = (2/r) \times [(dr/dz)/(M_1^2 - 1)]$. In the prediction that applies for a constant γ , the velocity distribution is computed from the local configuration of the wall. The requirement that the fluid velocity at the wall be parallel to the wall is not exactly satisfied because of the way in which the solution was obtained. The prediction from Eq. (3) is shown in Fig. 1 as curve e to be in close agreement with the Hall prediction and,

thus, the data in the throat vicinity of the 30°-15° nozzle. At the circular-arc-throat conical tangencies, the prediction is discontinuous because of d^2r/dz^2 ; these discontinuities are indicated by vertical dashed lines. Near the tangencies, the solution becomes more approximate, since the restrictions on the magnitude of the nozzle radius and its derivatives implied in the analysis are not satisfied.

The 45°-15° nozzle contour deviates even further from the restrictions imposed by this analysis; however, for comparison, this prediction is shown in Fig. 3 as curve e in a narrow part of the throat region. The rather sharp decrease in static pressure is predicted, but the prediction is below the data.

V. Static-Pressure Tap Size

The presence of a static-pressure hole causes some flow disturbance, which alters the measured static pressure from the true value. For sharp-edged holes, deeper than about 2 diam, measured static pressures in flows with negligible pressure gradients have been found to increase with hole size; it is believed that the small holes read nearer the true static pressure. Other effects, such as slight burrs and the presence of foreign particles, have been found to alter the readings as well. For nozzle flow, in addition to the pressure gradient induced in the flow by the presence of the hole, the external pressure gradient is superimposed in the flow direction. The flow disturbance is thus expected to increase with hole size because a larger pressure drop exists across the hole than when the freestream flow is not accelerating.

To investigate the effect of hole size on the static-pressure readings, the 2.51-1 nozzle shown in Fig. 2 was instrumented with 0.010- and 0.040-in.-diam tap pairs. As mentioned before, the holes were as sharp-edged as they could be made by smoothing with emery cloth any surface burrs that were produced by drilling. The ratio of hole depth to diameter was about 3. Static-pressure distributions were obtained over a range of stagnation pressures from 45 to 170 psia, with air at a stagnation temperature of 520°R (uncooled walls). Two of these distributions are shown in Fig. 4. To allow a direct comparison of the differences in the readings, the lower part of Fig. 4 also shows the percentage difference between the 0.010- and 0.040-in.-diam tap readings at locations where these two taps were axially within 0.002 in. of each other. This is the limit to which the axial location of the taps is known. As seen in Fig. 4, the pressure difference between the smallest and largest tap readings varies systematically through the nozzle; random differences (plus or minus) that would be associated with reading accuracy are not evident. The smallest tap has the lower reading, as has been observed in flows with negligible acceleration. The percentage difference in the tap readings is a maximum in the transonic region where the pressure gradient is largest. The difference is hardly discernible in the nozzle-inlet region where the freestream velocity is low and in the flow-separation region for the low-stagnation-pressure test where the reverse flow velocity is relatively low. The 0.002-in. uncertainty in the axial distance between the 0.010- and 0.040-in.-diam tap pairs would alter the percentage differences shown in Fig. 4 by 0.1 at most.

The trends of the differences shown for the two tests were typical of those found at intermediate stagnation pressures of 75, 100, and 125 psia, and duplicate tests at some of the pressures indicated the data to be reproducible. In a system in which pressure gradients can exceed those along the 2.51-1 nozzle, Jaivin¹⁴ found differences of the same magnitude as those shown in Fig. 4 for tap diameters ranging from 0.0016 to 0.019 in. by measuring the pressure distributions along a flat plate on which a liquid jet impinged. In that investigation, a limiting value of the tap size was found for which no further change in the measured pressure distribution was observed; a 0.004-in.-diam tap read the same as the 0.0016-in.-diam tap.

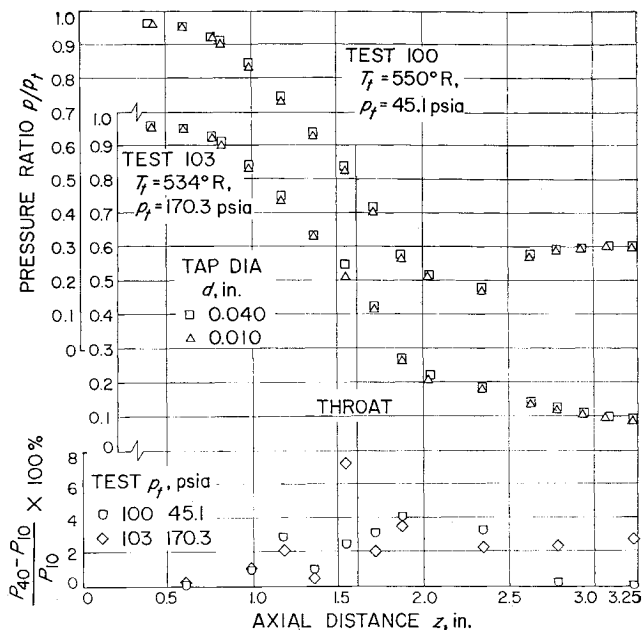


Fig. 4 Static-to-stagnation-pressure ratios along the 2.51-1 nozzle with different sized pressure taps.

To indicate the magnitude of the differences between the tap readings in another way, reference is made to an estimate of the static-pressure tap error. By dimensional analysis for a low-speed, essentially constant-property turbulent boundary layer with negligible flow acceleration, Livesey et al.¹⁵ and others give the error Δp for deep holes:

$$\Delta p/\tau = \frac{\Delta p}{\tau}(d^*)$$

where $d^* = d(\tau/\rho)^{1/2}/\nu$, d is the tap diameter, and τ is the wall shear stress. According to experimental measurements by Livesey et al. and others, $\Delta p/\tau$ increases monotonically with d^* to about 3 at $d^* \cong 900$, the limit at which measurements have been made. By comparison, in the throat region for the highest stagnation-pressure test, values of $(p_{40} - p_{10})/\tau$ are as large as 40; the corresponding value of d^* based on the 0.040-in.-diam tap is about 6200. For the lowest stagnation-pressure test, the predicted value in the throat region is less, $(p_{40} - p_{10})/\tau \cong 10$, as is the corresponding value $d^* \cong 1900$. In these estimates, the wall shear stress was predicted from the analysis of Ref. 8.

Unfortunately, since the true static pressure is not known, one can only conclude from the data shown in Fig. 4 that the static-pressure distributions shown in Figs. 1-3 are probably slightly higher than the true ones.

VI. Separation Pressures

For overexpanded nozzle operation, the ratios of separation to ambient pressure are shown in Fig. 5 for nozzles that have $r_c/r_{th} = 2.0$. There were too few pressure taps in the divergent region of the 45°-15° nozzle for a meaningful representation. The data are shown by the barred vertical lines. The upper bar is the tap reading upstream of the separation point; the lower bar would be that at the succeeding tap if separation had not occurred and was determined from higher stagnation-pressure tests. Thus, the actual value lies between the values shown. The Mach number at separation was calculated for isentropic flow ($\gamma = 1.4$) based on the average separation pressure. The ratios of separation-to-ambient pressure for the hot-flow tests with cooled walls (shaded symbols) are generally about 5 to 10% below the cold-flow values (open symbols). These lower values at the same stagnation pressure correspond to a relocation of the

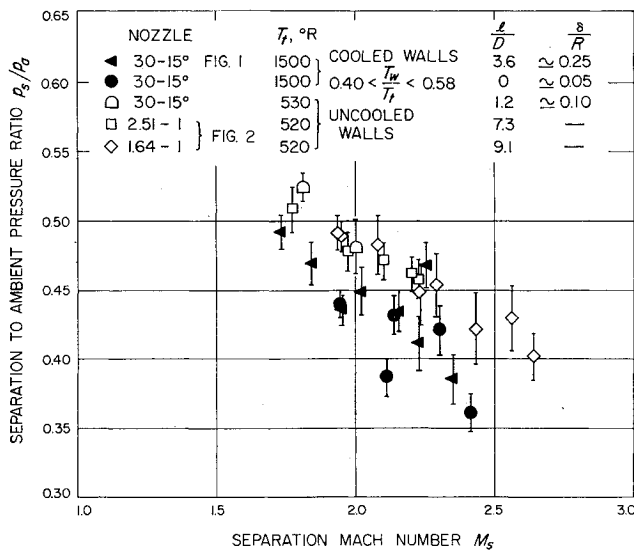


Fig. 5 Separation to ambient-pressure ratios for various nozzles.

separation point downstream with wall cooling, as was mentioned in Sec. III. This indicates that wall cooling is also important in the interaction between the shock wave and boundary layer which results in flow separation from the nozzle wall. Ahlberg et al.¹⁶ also found the same trend. For our data, it is not clear whether the lower separation pressures are due only to wall cooling, since, with hot flow and cooled walls, the boundary-layer-thickness Reynolds numbers at the separation point estimated from the analysis of Ref. 8 were about one-half of those for cold flow at the same stagnation pressure and boundary-layer thickness at the nozzle inlet. In this regard, the data shown in Fig. 5 for the 30°-15° nozzle with hot flow and cooled walls do not reveal any definite trend between the results with relatively thin boundary layers ($\delta/R \approx 0.05$) at the nozzle inlet and those with thicker layers ($\delta/R \approx 0.25$). However, it is difficult to determine whether there is any dependence on the boundary-layer-thickness Reynolds number, owing to the scatter of the results at the highest separation Mach numbers (last four shaded points), which correspond to separation near the nozzle-exit plane.

The data in Fig. 5 extend over rather low ratios of stagnation-to-ambient pressure because of the relatively small expansion-area ratios. When these data are compared with others obtained with uncooled walls, such as the accumulated results of Arens and Spiegler (Ref. 17, Fig. 2), the hot-flow data with a cooled wall are found to lie below those results.

VII. Flow Coefficients

In Fig. 6, comparisons between measured mass flow rate at a stagnation temperature of 1500°R (cooled walls) and computed values for 1-d isentropic flow ($\gamma = 1.35$) are shown in terms of the flow coefficient $c_d = \dot{m}/\dot{m}_1$. At the lower stagnation pressures, there is appreciable scatter in the values. Some of the scatter is undoubtedly due to errors in the mass flow-rate measurements. At the higher stagnation pressures, the scatter is less, and for both nozzles, the flow coefficient is approximately between 0.98 and 1.0. Since the flow through the nozzle region determines the mass flow rate through the nozzle, Fig. 6 also contains the Hall prediction:

$$c_d = \frac{\dot{m}}{\dot{m}_1} = 1 - (\gamma + 1) \left(\frac{r_{th}}{r_c}\right)^2 \left[96 - \frac{8\gamma + 21}{4608} \left(\frac{r_{th}}{r_c}\right) + \frac{754\gamma^2 + 1971\gamma + 2007}{552960} \left(\frac{r_{th}}{r_c}\right)^2 - \dots \right] \quad (4)$$

For the 30°-15° nozzle, the prediction from Eq. (4) is 0.9943, in fair agreement with the experimental values. This correspondence is expected from the close agreement of predicted and measured static pressures in the throat region. However, for the 45°-15° nozzle, the experimental values exceed the prediction from Eq. (4), in which only the first term in the brackets is retained. As mentioned before, the Hall solution diverges for $r_c/r_{th} < 1$. If only the first term in the brackets is included, the prediction is identical with that of either Sauer¹⁰ or Oswatitsch and Rothstein.¹³ Thus, the lower predicted values of the flow coefficient further show the inadequacy of existing predictions for nozzles with $r_c/r_{th} < 1$.

VIII. Thrust Ratios

To indicate how the nozzles tested would perform as thrust devices with negligible wall shear stresses, Fig. 7 shows ratios of actual thrust to that for 1-d isentropic flow ($\gamma = 1.40$) for a stagnation temperature of 1500°R (cooled walls):

$$\frac{F}{F_1} = \left[(pA)_i + \int_{A_i}^A p dA \right] / \left[(p_1 A)_i + \int_{A_i}^A p_1 dA \right] \quad (5)$$

To clearly illustrate the deviations, the nozzles are assumed to discharge into a vacuum, and the thrust ratios are shown for hypothetical expansion-area ratios from a value of 1 to that of the static-pressure tap location nearest the nozzle exit. The terms in the thrust expression represent the force on the nozzle-inlet area or effective chamber end wall and the integrated wall pressure distribution resulting in the axial force on the nozzle side wall. The shape of the thrust-ratio curve is dependent on whether the wall pressure is less or greater than the 1-d flow value and on the magnitude of the difference, as shown in Figs. 1 and 3. Shown for comparison is the often quoted correction factor $\frac{1}{2}(1 + \cos\theta)$ for nonaxial exit flow for conical nozzles. Thrust ratios for cold flow would be the same as those shown in Fig. 7, based on the data mentioned in Sec. III.

IX. Sonic Line

Table 1 contains a comparison at a stagnation temperature of 1500°R (cooled walls) of predicted and experimental location of the intersection of the sonic line with the edge of the boundary layer. The experimental values correspond to the point at which the Mach number obtained from the measured static-pressure distributions for isentropic flow ($\gamma = 1.35$)

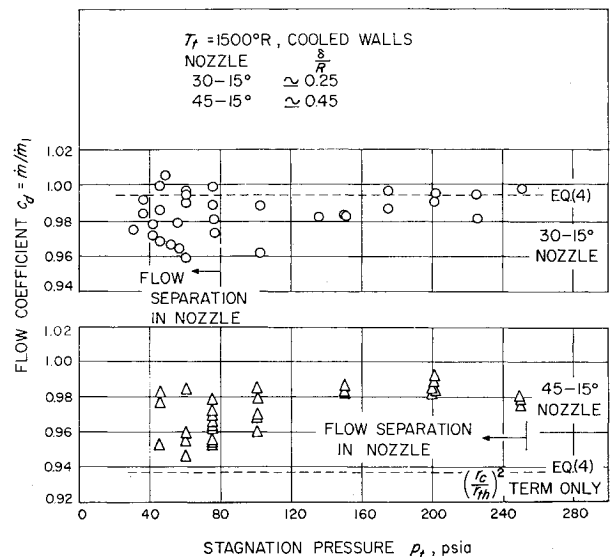


Fig. 6 Flow coefficients.

Table 1 Comparison of predicted and experimental sonic line intersection with edge of boundary layer at $T_t = 1500^\circ\text{R}$ (cooled walls)

Nozzle	$(\xi/r_{th})_{exp.}$	$(\xi/r_{th})_{Eq. (6)}$	$(\xi/r_{th})_{Hall}$
30°-15°	0.15-0.16	0.19	0.16
45°-15°	0.13-0.14	0.34	...

was equal to unity. One prediction for isentropic flow is from either Sauer¹⁰ or Oswatitsch and Rothstein.¹³

$$\xi/r_{th} = [(\gamma + 1)/2]^{1/2} (r_{th}/r_c)^{1/2} \quad (6)$$

where ξ is the axial distance upstream of the geometric throat. The other isentropic flow prediction is from Hall's analysis.⁹ For the 30°-15° nozzle, the prediction from Eq. (6) gives a value larger than that measured for the upstream distance to the sonic line, with better agreement afforded by Hall's prediction. Hall's analysis is not applicable to the 45°-15° nozzle, since $r_c/r_{th} < 1$; by using Eq. (6), the predicted distance is more than twice the experimentally deduced value. The cold-flow experimental values would be the same as those indicated in Table 1, based on the data mentioned in Sec. III.

X. Mass Flux Ratios

For the calculation of boundary-layer flow and heat transfer to nozzle walls, the local mass flux $(\rho V)_e$ at the edge of the boundary layer is needed. By assuming isentropic flow ($\gamma = 1.4$), this local mass flux was calculated from the measured static-pressure distributions and is shown non-dimensionalized by the 1-d isentropic flow value in Fig. 8. Through most of the nozzle, the local mass flux is less than the 1-d value, which implies lower wall heat fluxes, since for turbulent boundary-layer flows, $q \propto (\rho V)_e^{4/5}$. The mass flux deviation amounts to about 20% in the inlet region and just downstream of the throat for the 45°-15° nozzle; with the 30°-15° nozzle, the deviations are less.

The maximum values of the mass flux $(\rho V)_e$ occur just upstream of the throat at the intersection of the sonic line with the edge of the boundary layer. It is in this region that heat-transfer measurements indicate the maximum heat flux to the wall.^{1,6,18}

XI. Conclusions

Wall static-pressure measurements have been presented for air flowing through conical nozzles with circular-arc

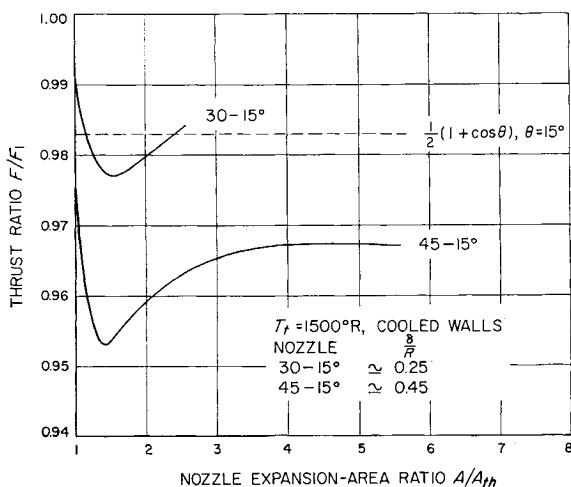


Fig. 7 Variation of thrust ratio with expansion-area ratio (curves were obtained from averaged p/p_1 ratios shown in Figs. 1 and 3).

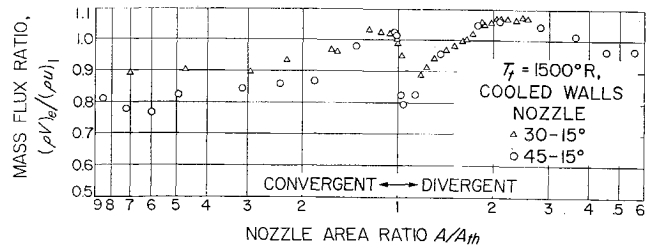


Fig. 8 Local to one-dimensional mass flux ratios along the nozzles (values were determined from averaged p/p_1 ratios shown in Figs. 1 and 3).

throats. Comparisons have been made with predictions. The results indicate the following.

- 1) In the throat region, where the flow is transonic, two-dimensional isentropic flow predictions are in close agreement with the data for the nozzles with a ratio of throat radius of curvature to throat radius $r_c/r_{th} = 2.0$, but inadequate for the nozzle with $r_c/r_{th} = 0.625$. Deviations as large as 30 and 45% from the simple one-dimensional isentropic flow prediction were found in the throat region for the nozzles with $r_c/r_{th} = 2.0$ and 0.625 , respectively.
- 2) Static-pressure measurements in the throat and divergent regions of nozzles with the same r_c/r_{th} and half-angle of divergence were found to be essentially independent of various inlet configurations.
- 3) Smaller deviations in static pressure from one-dimensional flow were found in the conical sections. In the convergence region, the magnitude increases with convergence angle, whereas in the divergence region, this effect was not investigated since all the nozzles tested had a 15° half-angle of divergence.
- 4) For underexpanded operation, the pressure measurements were insensitive to the effects of both cooled and uncooled walls and to nozzle-inlet boundary-layer thickness to 0.45 of the nozzle-inlet radius. Thus, boundary-layer effects were found to be negligible.
- 5) Pressure readings depend on tap size, with significant differences found between 0.010- and 0.040-in.-diam holes. The smallest tap reads the lower pressure, which is believed to be nearer the true static pressure.
- 6) For overexpanded nozzle operation, the separation point moved downstream with wall cooling for tests at the same stagnation pressure, so that the ratios of separation-to-ambient pressure for the hot-flow tests with cooled walls were generally about 5 to 10% below the cold-flow values.
- 7) Mass flow rate and thrust depend on the two-dimensionality of the flow through the transonic region, with boundary-layer effects relatively unimportant for the nozzles investigated that have expansion-area ratios to 6.6.
- 8) In the transonic region, local mass fluxes at the edge of the boundary layer deduced from the static-pressure measurements deviate less from one-dimensional flow values than do the static pressures. In the convergence section, the magnitudes of these deviations are about the same as they are in the transonic region and depend on the convergence angle.

References

- 1 Back, L. H., Massier, P. F., and Gier, H. L., "Convective heat transfer in a convergent-divergent nozzle," Intern. J. Heat Mass Transfer **7**, 549-568 (1964).
- 2 Scheller, K. and Bierlein, J. A., "Some experiments on flow separation in rocket nozzles," ARS J. **23**, 28-32, 40 (1953).
- 3 Frazer, R. P., Eisenklam, P., and Wilkie, D., "Investigation of supersonic flow separation in nozzles," J. Mech. Eng. Sci. **1**, 267-279 (1959).
- 4 Campbell, C. E. and Farley, J. M., "Performance of several conical convergent-divergent rocket-type exhaust nozzles," NASA TN D-467 (September 1960).
- 5 Arens, M. and Spiegler, E., "Separated flow in overex-

panded nozzles at low pressure ratios," Bull. Res. Council Israel **11C**, 45-55 (1962).

⁶ Fortini, A. and Ehlers, R. C., "Comparison of experimental to predicted heat transfer in a bell-shaped nozzle with upstream flow disturbances," NASA TN D-1743 (August 1963).

⁷ Stanton, T. E., "The variation of velocity in the neighborhood of the throat of a constriction in a wind channel," British Aeronautical Research Council R & M 1388 (1930).

⁸ Elliott, D. G., Bartz, D. R., and Silver, S., "Calculation of turbulent boundary-layer growth and heat transfer in axisymmetric nozzles," Jet Propulsion Lab. TR 32-387, Pasadena, Calif. (February 15, 1963).

⁹ Hall, I. M., "Transonic flow in two-dimensional and axially-symmetric nozzles," Quart. J. Mech. Appl. Math. **XV**, 487-508 (1962).

¹⁰ Sauer, R., "General characteristics of the flow through nozzles at near critical speeds," NACA TM-1147 (June 1947).

¹¹ Darwell, H. M. and Badham, H., "Shock formation in conical nozzles," AIAA J. **1**, 1932-1934 (1963).

¹² Migdal, D. and Landis, F., "Characteristics of conical supersonic nozzles," ARS J. **32**, 1898-1901 (1962).

¹³ Oswatitsch, K. and Rothstein, W., "Flow pattern in a converging-diverging nozzle," NACA TM-1215 (March 1949).

¹⁴ Jaivin, G. I., "Effect of hole size on pressure measurements made with a flat-plate dynamic-head probe," Jet Propulsion Lab. TR 32-617, Pasadena, Calif. (June 15, 1964).

¹⁵ Livesey, J. L., Jackson, J. D., and Southern, C. J., "The static hole error problem," Aircraft Eng. **XXXIV**, 43-47 (1962).

¹⁶ Ahlberg, J. H., Hamilton, S., Migdal, D., and Nilson, E. N., "Truncated perfect nozzles in optimum nozzle design," ARS J. **31**, 614-620 (1961).

¹⁷ Arens, M. and Spiegler, E., "Shock-induced boundary layer separation in overexpanded conical exhaust nozzles," AIAA J. **1**, 578-581 (1963).

¹⁸ Kolozsi, J. J., "An investigation of heat transfer through the turbulent boundary layer in an axially symmetric, convergent-divergent nozzle," Aerodynamic Lab., Ohio State Univ. TM-8 (July 1958).

SEPTEMBER 1965

AIAA JOURNAL

VOL. 3, NO. 9

Viscous, Radiating Shock Layer about a Blunt Body

H. HOSHIZAKI* AND K. H. WILSON†

Lockheed Missiles & Space Co., Palo Alto, Calif.

The effect of radiation cooling on the radiative and convective heat-transfer distribution around a blunt body is investigated. An integral method is employed to obtain solutions to the appropriate equations. The gas in the shock layer is assumed to be viscous, radiating but nonabsorbing. Solutions to the direct, viscous blunt-body problem are obtained by means of an iterative procedure. The results for a 30° hemisphere-cone show that the loss of energy in the shock layer by radiation reduces both the radiative and convective heat transfer. This reduction was found to persist around the body. It was also found that the entropy layer increased the radiative heating on the conical afterbody by two orders of magnitude.

Nomenclature

a_i = velocity profile coefficients
 b_i = enthalpy profile coefficients
 C_i = mass fraction of species
 C_p = total specific heat at constant pressure
 \bar{C}_p = frozen specific heat at constant pressure
 D_{ij} = diffusion coefficient for a multicomponent system
 \mathfrak{D}_{ij} = diffusion coefficient for a binary system
 E' = radiant emission per unit time per unit volume, $4\rho\lambda\sigma T^4$
 F_i = boundary-condition functions defined in Sec. 3.3
 f = velocity function, u/u_δ
 g = enthalpy function, H/H_δ
 h = static enthalpy
 h_i = static enthalpy of i th species, including enthalpy of formation
 H = total enthalpy
 I_1 = momentum integral
 I_2 = energy integral
 k = total thermal conductivity
 \bar{k} = frozen thermal conductivity
 m = exponent in Eq. (22a)
 M_i = molecular weight of species i
 n_i = moles of species i per unit volume
 n_t = total number of moles per unit volume
 P = static pressure
 Pr = total Prandtl number, $Pr = C_p\mu/k$
 \dot{q}_c = convective energy flux

\dot{q}_r = radiative energy flux
 r = body radius measured from body centerline
 R = body radius
 Re = Reynolds number, $\rho_\infty U_\infty R/\mu_\delta$
 Re_0 = Reynolds number, $\rho_{\delta,0} U_\infty R/\mu_{\delta,0}$
 S = distance along shock wave
 T = temperature
 \bar{T}_1 = reference temperature, 7200°K
 u = velocity component parallel to body
 U_∞ = freestream velocity
 \bar{U} = velocity in 10^4 fps
 v = velocity component normal to surface
 \bar{v} = velocity component normal to surface in shock-oriented coordinate system
 X_i = mole fraction of species i , $X_i = n_i/n_t$
 x, y = body-oriented coordinate system
 β = velocity gradient
 γ = isentropic index
 δ = shock-detachment distance
 $\bar{\delta}$ = transformed shock-detachment distance, Eq. (5d)
 δ_b = boundary-layer thickness
 ϵ = difference between body and shock angle, also emissivity
 η = Dorodnitsyn variable, Eq. (8a)
 θ = body angle
 κ = body curvature
 $\bar{\kappa} = 1 + \kappa y$
 λ = mass absorption coefficient
 $\bar{\lambda}_t$ = reference mass absorption coefficient, 96.8 ft²/slug
 μ = dynamic viscosity
 ν = kinematic viscosity
 ρ = density
 $\bar{\rho}$ = density ratio across shock, ρ_∞/ρ_δ
 σ = Stefan-Boltzmann constant
 ϕ = shock angle
 ω = vorticity

Presented at the AIAA Entry Technology Conference, Williamsburg and Hampton, Va., October 12-14, 1964 (no preprint number; published in bound volume of preprints of the meeting); revision received May 5, 1965.

* Staff Scientist, Aerospace Sciences Laboratory. Member AIAA.

† Research Scientist, Aerospace Sciences Laboratory. Member AIAA.